https://doi.org/10.1016/j.sse.2017.09.008

Ni antidot structure via single-step anodization of Al/Ni films

Sheung Mei Ng[a], Wang Cheung Wong[a], Xu Fang[b], Hui Ye[b], Chi Wah Leung[a]*

[a]Department of Applied Physics, The Hong Kong Polytechnic University, Hung Hom, Kolwoon, Hong Kong

[b]State Key Laboratory of Modern Optical Instrumentation, Department of Optical Engineering, Zhejiang University, Hangzhou, 310027, P. R. China

*Email: dennis.leung@polyu.edu.hk

Tel: 852-27665670

Abstract

Antidot nanostructures were fabricated on Ni films by a single-step anodization process of magnetron-sputtered Al/Ni/W trilayers. Coercivity and saturation magnetization of the Ni layer were tuned by controlling the anodization time. Transmission electron microscopy was used to investigate the mechanism of the antidot formation process. The present study provides a simple and direct route for the fabrication of magnetic antidot nanostructures for device applications.

Highlights

- Anodization of Al/Ni/W films in acidic electrolyte gives antidot Ni layer.

- Coercivity and saturation magnetization behaviour is controlled by anodization time.

- Possible mechanisms of antidot formation in Ni layer suggested.

Keywords:

Antidot structure, anodization

1. Introduction

Magnetic nanostructures are of immense interests due to their potential for various applications, ranging from magnetic storage media [1, 2], memory cells [3], logic operations [4], among many others. For example, magnetic antidot structures, which are magnetic plain films with holey patterns, have been prepared and investigated for both memory [5] and magnonic crystal studies [6]. The magnetic properties of the antidot structure, such as coercivity and magnetoresistance behaviour, can also be controlled by the dimensions of the pores [7, 8]. Such a structure becomes a promising candidate participating in electronic device research such as transistors, magnetic field-effect transistor (MAGFET) chipsets and recording media; the continuous nature of antidot array naturally surpasses the superparamagnetic limit that is otherwise present in dot patterns [2, 9-11].

Various techniques have been employed in the preparation of magnetic antidot structures. Patterns in micrometre scales can be prepared by photolithography [12]. For nanoscale antidot features, one generally resorts to techniques such as focused-ion beam lithography and electron-beam lithography [7, 13, 14]. However these methods of nanoscale pattern fabrication involve expensive equipment and long processing time due to their serial nature of patterning.

Antidot magnetic nanostructures were reported to be prepared by depositing magnetic films on top of porous anodic aluminium oxide (AAO) templates [15-17]. An enhancement of coercivity and magnetoresistance was observed as compared with the plain magnetic films. With the magnetic materials prepared on the top of AAO pores, however, the effect of AAO template surface roughness on the magnetic properties of the antidot films cannot be ignored. In addition, the thickness of the magnetic film that can be deposited is limited, as thick films would seal off the pores and result in continuous film structures.

Here we report the preparation of antidot structure by direct anodization of Al/Ni/W trilayer films. Transmission electron microscopy confirmed the growth of antidot structures. An enhanced coercivity was observed in samples with the anodization process extending into the Ni layer. Tunable coercivity was achieved by simply controlling the anodization time. The technique presented here offers a simple, cost-effective route for the preparation of magnetic antidot nanopatterns.

2. Experimental details

Trilayer films of Al (300 nm)/Ni (10 nm)/W (25 nm) were prepared on SiO_2/Si substrates by dc magnetron sputtering. In the trilayer structure, tungsten works as the adhesion layer and to quench the anodization process [18]. Thin Al layers were used to enhance the uniformity of anodization in Al (and hence Ni), although thick Al layers are generally used for inducing regular arrangement of pores [19, 20]. Si substrates were cleaned in ultrasonic baths of acetone and ethanol successively for at least 10 minutes, before they were loaded into the sputtering chamber and evacuated to a base pressure of $1x10^{-4}$ Pa or better. Film deposition was carried out at room temperature. The tungsten layer was deposited with 0.8 Pa Ar, while Ni and Al layers were deposited in an Ar pressure of 0.2 Pa. All of the layers were prepared with dc power of 70 W. For control purpose, anodization processes were also performed in Al foils (100 μm) and sputter-deposited Al (~1 μm)/W (25 nm)/Ti (25 nm) trilayer samples, using identical anodization conditions.

Constant voltage anodization processes were performed on the samples at 7^oC in 0.17M H_3PO_4 solutions [21]. A LabVIEW programme was used to control the voltage ramping at 1 Vs^{-1} at the beginning of the anodization process, and to maintain the constant voltage of 170 V while monitoring the current flow in the circuit for the estimation of current density. A voltage ramp was used instead of directly applying a high voltage to the samples, in order to avoid the detachment of the film from the substrate due to the sudden current surge and vigorous reactions. A constant voltage was maintained once it was ramped to the target value. The acidic electrolyte was stirred vigorously throughout the process to promote ion diffusion. Magnetic properties of the samples were studied with vibrating sample magnetometer (VSM) (Lakeshore 7407). Cross-sectional morphologies of the samples were studied with transmission electron microscope (TEM) (Jeol JEM-2100F).

3. Results and discussions

Fig. 1 (a) to (c) show the current density-time curves for the anodization of Al foil (100 μm), Al/W/Ti and Al/Ni/W samples, respectively; the first two types of samples are control runs for comparison purposes. When the voltage is ramped up from 0 to 170 V, there is an increase of current because the aluminium oxide formed on the surface is quickly dissolved by the increasing voltage. Once the constant voltage of 170 V is reached, the current density

drops due to the continuous formation of aluminium oxide. If there is sufficient Al for sustaining the anodization process, there is a competition between oxide formation (governed by the strong electric field which drives the movement of oxygen-containing anions towards Al) and alumina dissolution (field-assisted dissolution and thermal-assisted dissolution); a dynamic equilibrium of oxide formation process is eventually achieved, during which a steady current density would be recorded (Fig. 1(a)) [22, 23]. In the cases of Al foil (Fig. 1(a)) and Al film (Fig. 1(b)), only one current peak can be observed in the corresponding current density-time curves, which is attributed to the ramping of voltage at the beginning of reaction.

On the other hand, due to the limited thickness of Al layer in our current study, there is insufficient time for the aluminium anodization process to reach a steady state before the Al layer is completely consumed, as evident from the current density-time curve that is on the decreasing trend (Fig. 1(b)). It is noted that for the Al/Ni/W trilayer, two additional current peaks that can be observed at the later part of the reaction apart from the ramping voltage peak in the Al layer (Fig. 1 (c)); these two peaks correspond to the stages of anodization reaching the Ni and W layers, respectively. The increase of current indicates the exposure of a conducting (metallic) layer to the electrolyte, while decreasing current indicates the formation of oxide or the exposure of the insulating substrate (SiO_x) surface. It is therefore the first indication that the Ni layer is oxidized. The increase of current after consuming the Al film has also been reported in other film structures such as Al/Si and Al/Ti/Si, due to the oxidation of underlying conductive material [24]. Once the oxidation progresses into these layers, the competing processes of anodization and oxide dissolution lead to the gradual drop of the recorded current, similar to the case of Al anodization. We also note here that the sharp spikes in the current-time graphs (e.g. around 1800 s in Fig. 1(c)) arise typically from the exposure of metal layers due to the localized delamination of the film, as a consequence of gas bubble formation during the reaction.

Anodization of Ni into NiO_x, as evident from the current density-time curve, may affect its intrinsic magnetic properties. To this end, samples with different anodization times were prepared for investigating their magnetic responses. We assigned the instance at which the reaction reaching the Ni layer and achieving the current peak as $t = 0$, with the time before (after) this point assigned as negative (positive). Table 1 summaries the anodization

time for different Al/Ni/W samples (A to H) prepared in this work, with the accompanying current density-time curve illustrating the particular moment at which the reaction is terminated for each sample.

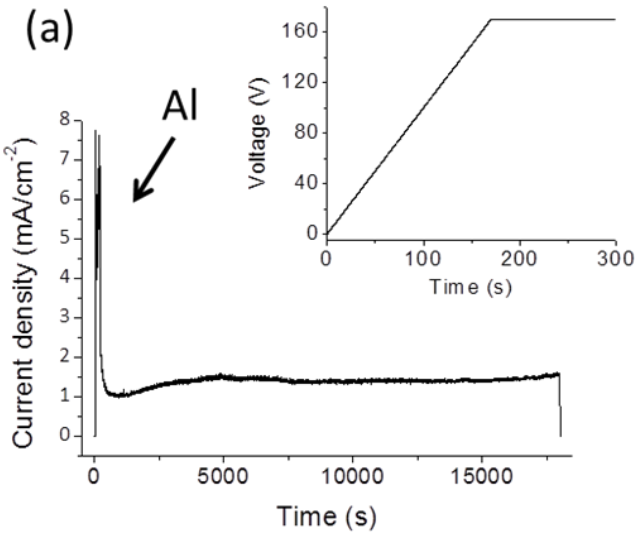
(a)
Al
Current density (mA/cm-2)
Time (s)
Voltage (V)
Time (s)

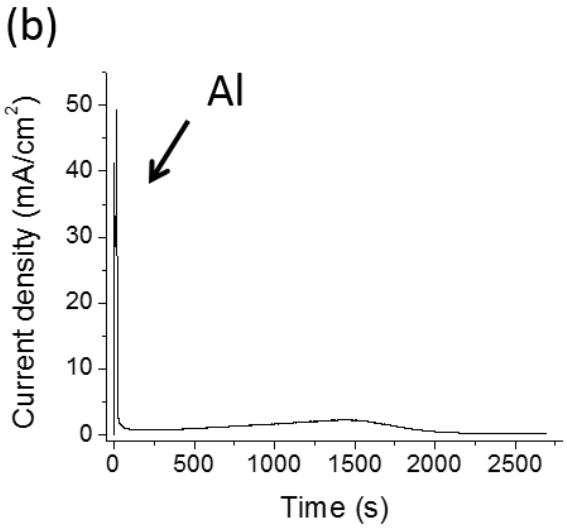
(b)
Al
Current density (mA/cm2)
Time (s)

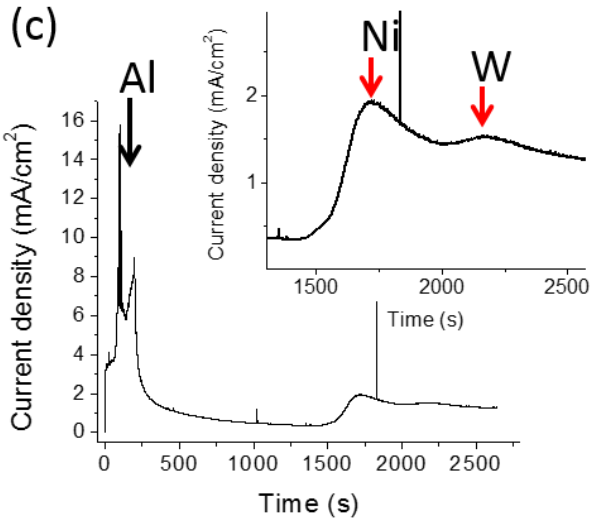
(c)
Al
Ni
W
Current density (mA/cm2)
Time (s)
Current density (mA/cm2)
Time (s)

Fig. 1. Current density-time curves of aluminium anodization in 0.17 M H_3PO_4 at 170 V. (a) Anodization of aluminium foil, which shows a typical peaked behaviour. Inset of (a): voltage profile for anodization of all the samples in this work. (b) Anodization of Al/W/Ti. (c) Anodization of Al/Ni/W. Inset of (c): magnified current density-time curve in (c), showing the two peaks which appear during the anodization of Al/Ni/W film apart from the main Al anodization peak.

Sample Name	**Anodization time *t* (min)**	**Remarks**
Un-anodized trilayer sample	Not applicable	Control sample
A	-20	AAO formation under progress, before reaching Ni layer
B	0	The most vigorous reaction in the Ni layer
C	+2	
D	+4	The most vigorous reaction in the W layer
E	+7	
F	+15	
G	+60	
H	+180	

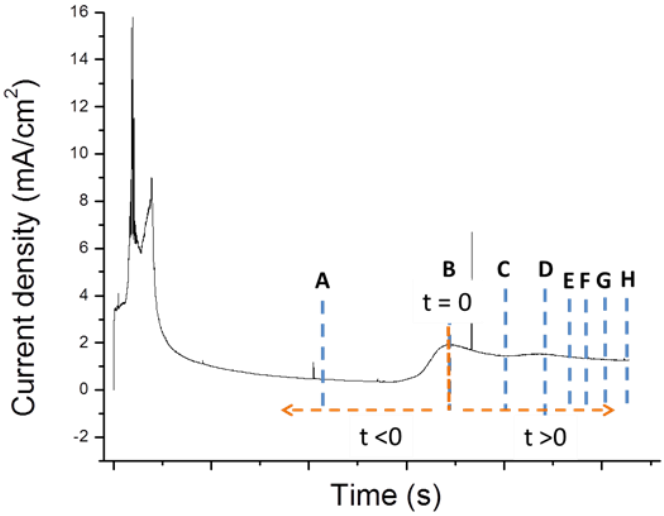

Table 1. Al/Ni/W film anodization samples prepared in this work, with the moment at which the reaction terminates for each sample indicated in the accompanying current density-time curve.

Magnetic properties of the samples in Table 1 were measured by VSM at room temperature, and the results are shown in Fig. 2. The unanodized trilayer sample shows the narrowest hysteresis loop and the strongest

magnetization, while the loops widen and show reduced magnetization with increasing anodization time. Coercivity and magnetization of the samples (normalized against the unanodized trilayer sample's value) were extracted from the loops and are shown Fig. 2(b) and (c) respectively, with the black dashed lines in these figures representing the coercivity and magnetization of the unanodized trilayer sample. It is found that the coercivity (Fig. 2 (b)) of the samples increases with the anodization time, while the saturation magnetization decreases (Fig. 2 (c)) upon anodization reaction.

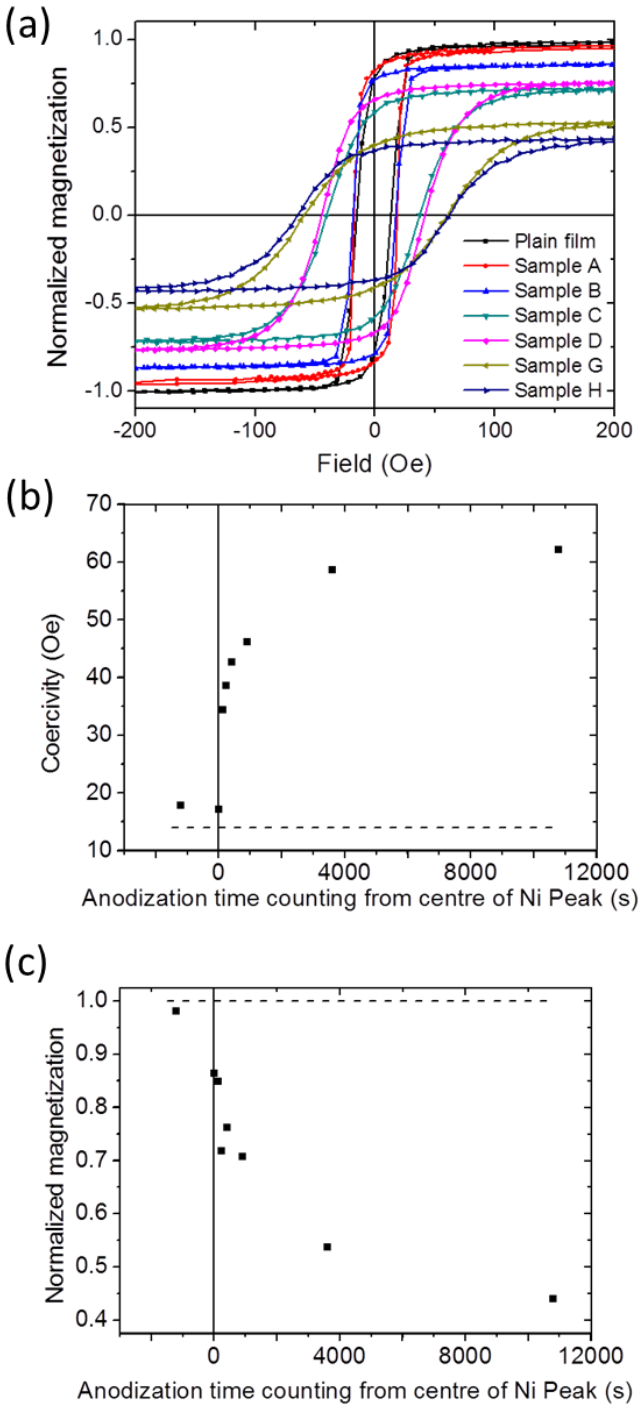

Fig. 2. (a) Magnetic hysteresis loop of Al/Ni/W films with different anodization time. Plots of coercivity and normalized magnetization, as a function of anodization time *t*, are shown in (b) and (c) respectively (*t* = 0 correspond to the Ni anodization peak in the current density-time curve, see Fig. 1(c)).

The change in the magnetic properties of the samples with anodization time is attributed to the antidot structure formation in the Ni layer and the formation of NiO_x. The 10-nm thick Ni layer is not chemically inert, and it is possible for ions in the electrolyte to pass through the AAO barrier layer and react with Ni. To verify this assumption, cross-sectional TEM was prepared for Sample G (Fig. 3(a)). While the AAO pore structure can be clearly seen, pillars comprising nanocrystals in an amorphous matrix are observed at the bottom of each pore. Energy-dispersive x-ray spectroscopy (EDX) analysis at the pillar region (Fig. 4(b), to be discussed in details, shows only the presence of Ni, Al and O, hence eliminating the possibility of W or WO_x in the region. In fact, anodization for WO_x exhibits completely different morphology, as evident from cross-section TEM image of the anodized Al/W/Ti sample (Fig. 3(b)), where no nanocrystal structure can be observed within the WO_x. On the other hand, AlO_x formed by anodization process is amorphous, as shown in the TEM image of the AAO wall in Fig. 3(a) and (b). However, as shown by EDX analysis, the atomic percentage ratio of oxygen to aluminium obtained from the pillar region (Fig. 4(a), O:Al = 1.14 : 1) is higher than that obtained from AAO wall (Fig. 4(b), O:Al = 0.46 : 1). Hence, the detected oxygen cannot come solely from AlO_x, meaning that NiO_x must be present in the matrix-crystal composite observed in Fig. 3(a). Fig. 3(c) shows the high resolution TEM image, with *d*-spacing measured from the nanocrystal structure being 2.06Å, which is closer to the reported value for NiO (200) crystal plane [25]. Diffraction pattern obtained from the pillar region shows both amorphous ring and diffraction spot pattern, the latter of which can be assigned to NiO (200) plane; we note with caution that although the measured crystal spacings are assigned to those of NiO, the nickel oxide obtained through the anodization process is likely to be non-stoichiometric. Our TEM results therefore also support the formation of NiO_x. The antidot structure formed is schematically shown in Fig. 3(d), which consists of the Ni antidot film formed by the sequential anodization of Al and Ni, and the holey regions are filled with NiO_x. A definitive proof of NiO_x formation and its exact morphology can be provided by localized X-ray photoelectron spectroscopy (XPS) or element-specific imaging techniques (such as electronic-energy loss spectroscopic (EELS) imaging [26]).

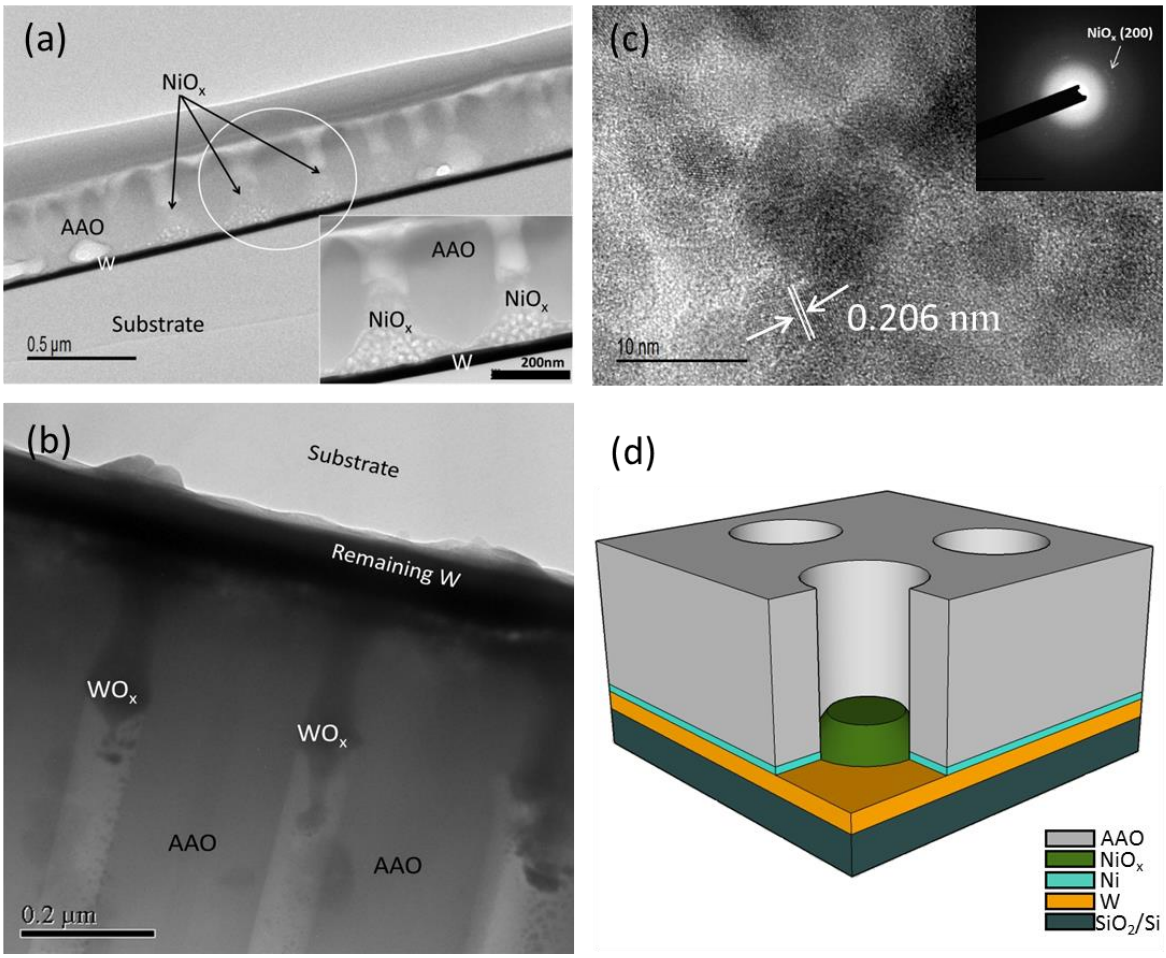

Fig. 3. (a) Cross-sectional TEM image of Al/Ni/W film anodized for one hour beyond the Ni peak (Sample G), showing the formation of NiO_x in AAO pore. Inset: close-up of the circled region. (b) TEM image of amorphous WO_x formed by anodization of Al/W/Ti film. (c) High resolution TEM image of nanocrystals embedded in the amorphous matrix within the AAO pore shown in (a). Inset shows the selected-area diffraction pattern of the region. (d) Schematic diagram illustrating the formation of Ni antidot with the hole filled by NiO_x.

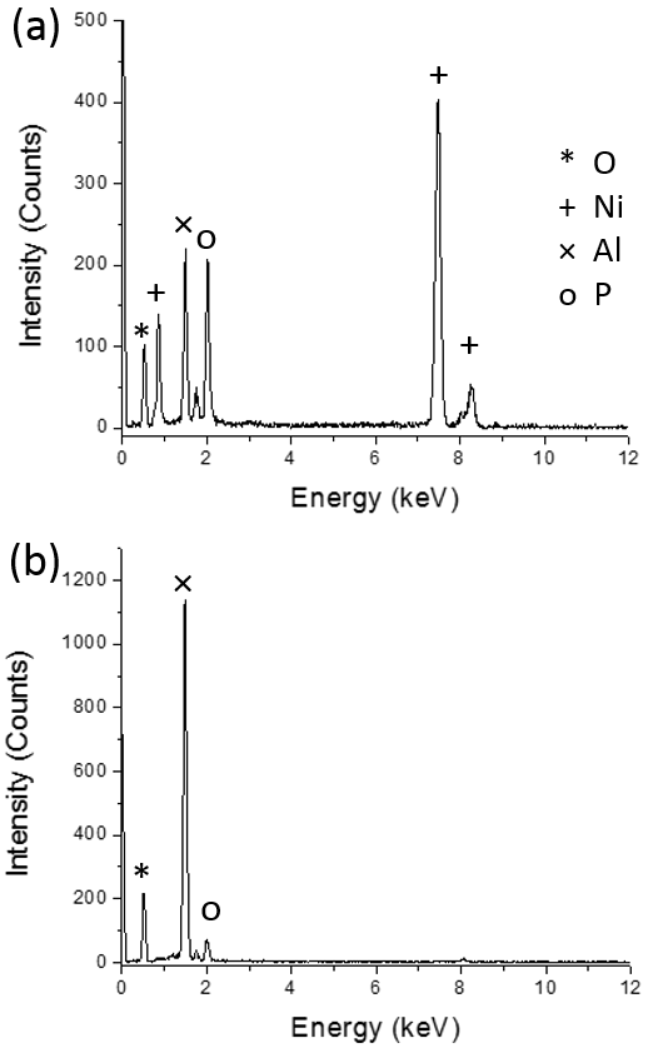

Fig. 4. Energy-dispersive x-ray spectra at (a) the pillar region and (b) at AAO wall. The corresponding peaks for Al, Ni and O are labelled in the figures. No characteristic peaks for W is observed, and P is detected as residuals of the electrolyte used for the anodization process.

With the aid of TEM results, the change of magnetic properties is discussed as follows. The formation of antidot structure in the Ni layer acts as pinning sites that impede the domain wall motion, resulting in the increase of coercivity [16, 17, 27]. On the other hand, the formation of antiferromagnetic NiO_x, also can lead to localized pinning of the Ni/NiO_x interface through exchange bias effect [28]. It is well-known that exchange biased systems can lead to a shift of hysteresis loop, generally accompanied by an enhanced coercivity [29]. Low temperature VSM was carried at 100 K for sample G, after field cooling from 370 K at 10-

kOe external field. No shifting of the hysteresis loop centre was observed. This may be due to the small contact area between NiO_x and Ni (edges of antidots) as compared with the volume of the Ni antidot film. The effect of Ni antidot formation and the NiO_x formation both enhanced the coercivity and cannot be distinguished with the current results. On the other hand, the reduction of measured magnetization is a result of Ni metal losses by either NiO_x formation or dissolving of Ni into the acid electrolyte by prolonged anodization process.

In our trilayer film structure, it is possible to transfer the Al/Ni film to other substrates and expose the Ni film by dissolving the WO_x layer with buffer solutions (pH = 7.00) [18]. The neutral solution selectively etches WO_x while keeping the structure of AAO and Ni intact. This provides the option of exposing Ni antidot film for specific applications. Besides, with AAO growing on the top of Ni layer, the dimensions of Ni antidots such as diameter and spacing of the holes can be tuned by controlling the anodization process [15], which have been well-studied; this in turn controls the magnetic properties of Ni layer. The anodization of the proposed film structure thus shows a high tunability and flexibility on the magnetic properties of Ni antidot layer.

4. Conclusion

Magnetic properties of antidot Ni layer can be tuned by a simple method of single-step anodization on Al/Ni/W films. Coercivity was increased and saturation magnetization was reduced by increasing the anodization time. Our study showed a single-step direct patterning of magnetic antidot films. The technique can be easily extended to the fabrication of regular pore arrays of designated geometries by a simple prepatterning process [21], thus further increasing the versatility of the technique.

Acknowledgement

This work was supported by the University Grants Committee of the Hong Kong Special Administrative Region (UGC, HKSAR (PolyU 153015/14P)) and the Hong Kong Polytechnic University (PolyU (G-YM43, A-PM21)).

References

[1] Dong Q, Li G, Ho C-L, Leung C-W, Pong PW-T, Manners I, et al. Facile Generation of L10-FePt Nanodot Arrays from a Nanopatterned Metallopolymer Blend of Iron and Platinum Homopolymers. Adv Funct Mater. 2014;24:857-62.
[2] Ross CA. Patterned Magnetic Recording Media. Annu Rev Mater Res. 2001;31:203-35.
[3] Chen E, Apalkov D, Diao Z, Driskill-Smith A, Druist D, Lottis D, et al. Advances and Future Prospects of Spin-Transfer Torque Random Access Memory. IEEE Trans Magn. 2010;46:1873-8.
[4] Cowburn RP, Welland ME. Room Temperature Magnetic Quantum Cellular Automata. Science. 2000;287:1466-8.
[5] Cowburn RP, Adeyeye AO, Bland JAC. Magnetic domain formation in lithographically defined antidot Permalloy arrays. Appl Phys Lett. 1997;70:2309-11.
[6] Neusser S, Duerr G, Tacchi S, Madami M, Sokolovskyy ML, Gubbiotti G, et al. Magnonic minibands in antidot lattices with large spin-wave propagation velocities. Phys Rev B. 2011;84:094454.
[7] Wang CC, Adeyeye AO, Singh N. Magnetic antidot nanostructures: effect of lattice geometry. Nanotechnology. 2006;17:1629-36.
[8] Papaioannou ET, Kapaklis V, Patoka P, Giersig M, Fumagalli P, Garcia-Martin A, et al. Magneto-optic enhancement and magnetic properties in Fe antidot films with hexagonal symmetry. Phys Rev B. 2010;81:054424.
[9] Michea S, Palma JL, Lavín R, Briones J, Escrig J, Denardin JC, et al. Tailoring the magnetic properties of cobalt antidot arrays by varying the pore size and degree of disorder. J Phys D: Appl Phys. 2014;47:335001.
[10] Moore LS, Goldhaber-Gordon D. Low-dimensional physics: Magnetic lattice surprise. Nat Phys. 2007;3:295-6.
[11] Leitao DC, Ventura J, Pereira AM, Sousa CT, Moreira JM, Carpinteiro FC, et al. Study of Nanostructured Array of Antidots Using Pulsed Magnetic Fields. J Low Temp Phys. 2010;159:245-8.
[12] Yu C, Pechan MJ, Mankey GJ. Dipolar induced, spatially localized resonance in magnetic antidot arrays. Appl Phys Lett. 2003;83:3948-50.
[13] Castán-Guerrero C, Herrero-Albillos J, Bartolomé J, Bartolomé F, Rodríguez LA, Magén C, et al. Magnetic antidot to dot crossover in Co and Py nanopatterned thin films. Phys Rev B. 2014;89:144405.
[14] Neusser S, Duerr G, Tacchi S, Madami M, Sokolovskyy ML, Gubbiotti G, et al. Magnonic minibands in antidot latticeswith large spin-wave propagation velocities. Phys Rev B. 2011;84:094454.
[15] Navas D, Ilievski F, Ross CA. CoCrPt antidot arrays with perpendicular magnetic anisotropy made on anodic alumina templates. J Appl Phys. 2009;105:113921.
[16] Xiao ZL, Han CY, Welp U, Wang HH, Vlasko-Vlasov VK, Kwok WK, et al. Nickel antidot arrays on anodic alumina substrates. Appl Phys Lett. 2002;81:2869.
[17] Badini Confalonieri GA, Pirota KR, Vazquez M, Nemes NM, Garcia-Hernandez M, Knobel M, et al. Magnetic and transport properties in ordered arrays of permalloy antidots and thin films. J Appl Phys. 2010;107:083918.
[18] Oh J, Thompson CV. Selective Barrier Perforation in Porous Alumina Anodized on Substrates. Adv Mater. 2008;20:1368-72.
[19] Shingubara S, Okino O, Murakami Y, Sakaue H, Takahagi T. Fabrication of nanohole array on Si using self-organized porous alumina mask. J Vac Sci Technol B. 2001;19:1901-4.

[20] Li F, Zhang L, Metzger RM. On the Growth of Highly Ordered Pores in Anodized Aluminum Oxide. Chem Mater. 1998;10:2470-80.
[21] Ng SM, Wong HF, Lau HK, Leung CW. Large-Area Anodized Alumina Nanopore Arrays Assisted by Soft Ultraviolet Nanoimprint Prepatterning. J Nanosci Nanotechnol. 2012;12:6315-20.
[22] Su Z, Zhou W. Formation Mechanism of Porous Anodic Aluminium and Titanium Oxides. Adv Mater. 2008;20:3663-7.
[23] Su Z, Hahner G, Zhou W. Investigation of the pore formation in anodic aluminium oxide. J Mater Chem. 2008;18:5787-95.
[24] Wu MT, Leu IC, Hon MH. Anodization behavior of Al film on Si substrate with different interlayers for preparing Si-based nanoporous alumina template. J Mater Res. 2004;19:888-95.
[25] Li Y, Afzaal M, O'Brien P. The synthesis of amine-capped magnetic (Fe, Mn, Co, Ni) oxide nanocrystals and their surface modification for aqueous dispersibility. J Mater Chem. 2006;16:2175-80.
[26] Arenal R, de la Peña F, Stéphan O, Walls M, Tencé M, Loiseau A, et al. Extending the analysis of EELS spectrum-imaging data, from elemental to bond mapping in complex nanostructures. Ultramicroscopy. 2008;109:32-8.
[27] Torres L, Lopez-Diaz L, Iñiguez J. Micromagnetic tailoring of periodic antidot permalloy arrays for high density storage. Appl Phys Lett. 1998;73:3766-8.
[28] Nogués J, Schuller IK. Exchange bias. J Magn Magn Mater. 1999;192:203-32.
[29] Leung CW, Blamire MG. Interaction between exchange-bias systems in $Ni_{80}Fe_{20}$ / $Fe_{50}Mn_{50}$ / Co trilayers. Phys Rev B. 2005;72:054429.